Journal of
Applied Crystallography
ISSN 0021-8898

Received 27 July 2011
Accepted 18 September 2011

The *LaueUtil* toolkit for Laue photocrystallography. I. Rapid orientation matrix determination for intermediate-size-unit-cell Laue data

Jarosław A. Kalinowski,[a,b]* Anna Makal[a] and Philip Coppens[a]

[a]Chemistry Department, University at Buffalo, State University of New York, Buffalo, NY 14260-3000, USA, and [b]Physical Biosciences Division, Lawrence Berkeley National Laboratory, Berkeley, CA USA. Correspondence e-mail: jak@kalinowscy.eu

A new method for determination of the orientation matrix of Laue X-ray data is presented. The method is based on matching of the experimental patterns of central reciprocal lattice rows projected on a unit sphere centered on the origin of the reciprocal lattice with the corresponding pattern of a monochromatic data set on the same material. This technique is applied to the complete data set and thus eliminates problems often encountered when single frames with a limited number of peaks are to be used for orientation matrix determination. Application of the method to a series of Laue data sets on organometallic crystals is described. The corresponding program is available under a Mozilla Public License-like open-source license.

1. Introduction

Although the Laue method is intrinsically related to the discovery of X-ray diffraction, it was in the decades following that discovery largely replaced by monochromatic techniques, which provided more accurate crystallographic data. However, with the development of pump–probe time-resolved (TR) diffraction experiments, other considerations have become important. Owing to the mismatch between the repeat rate of powerful laser pump sources and that of the pulsed X-ray sources, only a small fraction of the flux available at synchrotron sources can be used. As Laue diffraction uses a broader bandpass, it makes more efficient use of the available photons. It has therefore undergone a revival, not only in TR macromolecular studies (Moffat, 2001; Šrajer *et al.*, 2000; Anderson *et al.*, 2004) but also in small-molecule systems of chemical importance (Coppens, 2011; Makal *et al.*, 2011).

Early determinations of the orientation matrix from Laue patterns were based on the calculation of the angles between the scattering vectors of one or a few pairs of observed reflections and the comparison of these angles with the angles between reciprocal space vectors based on the known cell dimensions, as summarized by Laughier & Filhol (1983). A similar method based on the angles between zone axes was described by Hart & Rietman (1982). The need for rapid and systematic orientation matrix determination for Laue data was addressed by Jacobson (1986) with specific emphasis on neutron time-of-flight measurements in which the wavelength of the observed reflections is known. The Daresbury software suite (Helliwell *et al.*, 1989) for Laue indexing is applicable to patterns that contain well populated arcs of reflections so that prominent zone axes can be identified by searching for their intersections. More recent developments often involve gnomonic projections and introduce user interfaces and search automation (Campbell, 1995; Carr *et al.*, 1992; Wenk *et al.*, 1997). A different method, also based on geometrical pattern matching, was presented in the context of micro-Laue diffraction studies. It determines the orientation matrix of a diffracting volume by maximizing a normalized cross-correlation index between experimental and theoretical image patterns (Gupta & Agnew, 2009).

In a more direct approach we revert to a method based on the angles between the reciprocal lattice vectors of strong reflections, making optimal use of the now available computer power. This technique uses the whole data set and thus eliminates the necessity of manually examining raw frames in search of the 'best' candidate to obtain an initial guess of the orientation matrix, unlike the procedure required by single-frame-oriented indexing software. The whole-data-set approach is particularly advantageous in the case of photocrystallographic measurements using a pink-beam synchrotron source, in which case the combination of a narrow radiation spectrum and very small sample sizes leads to a small number of spots per frame. Because of limited high-order scattering this number cannot be increased by a decrease in the sample-to-detector distance.

This paper focuses on the determination of the orientation matrix. Indexing of the diffraction spots will be described in a separate publication.

2. The method

The orientation matrix determination described below requires two assumptions to be met in order to be applicable. First, the exact experimental geometry, including goniometer rotation angles and detector characteristics, must be known. This excludes application of the method when either different

crystals are measured on each frame (liquid-jet injection technique) or for some other reason the crystal has moved unexpectedly. The second assumption is that the crystal cell parameters and approximate structure factors are known. This essentially means that an experiment using a monochromatic X-ray beam must be performed in advance in order to obtain reference data. While this requirement is indeed limiting, in the context of photocrystallography in which this method was developed it is always fulfilled to a sufficient accuracy. Moreover, our preliminary studies indicate that it is possible to modify the approach presented here in order to eliminate the need for reference data.

The method does not require knowledge of the beam spectral distribution (the λ curve) nor does it attempt to estimate one from the data.

2.1. Problem formulation

Each spot on the detector can be related to one, or in the case of the Laue technique more than one, reciprocal-lattice point *hkl*.

The position of the lattice point is expressed using reciprocal unit-cell vectors as

$$\mathbf{h} \equiv \mathbf{h}_{hkl} = h\mathbf{a}^* + k\mathbf{b}^* + l\mathbf{c}^*. \quad (1)$$

The same vector can be expressed in Cartesian coordinates in either laboratory (L) or goniometer-head-fixed (g) coordinate systems:

$$\mathbf{h} = x_\mathrm{L}\hat{\mathbf{x}}_\mathrm{L} + y_\mathrm{L}\hat{\mathbf{y}}_\mathrm{L} + z_\mathrm{L}\hat{\mathbf{z}}_\mathrm{L} = x_\mathrm{g}\hat{\mathbf{x}}_\mathrm{g} + y_\mathrm{g}\hat{\mathbf{y}}_\mathrm{g} + z_\mathrm{g}\hat{\mathbf{z}}_\mathrm{g}, \quad (2)$$

where x_L, y_L, z_L and $\hat{\mathbf{x}}_\mathrm{L}$, $\hat{\mathbf{y}}_\mathrm{L}$, $\hat{\mathbf{z}}_\mathrm{L}$ are coordinates and axial unit vectors defining the laboratory system, described in Appendix *A*, and similarly x_g, y_g, z_g and $\hat{\mathbf{x}}_\mathrm{g}$, $\hat{\mathbf{y}}_\mathrm{g}$, $\hat{\mathbf{z}}_\mathrm{g}$ are analogous quantities in the goniometer-head-fixed system. The two sets of coordinates can be related *via* the $\mathbf{\Phi}_\varphi$ matrix describing the rotations of the goniometer head:

$$\begin{pmatrix} x_\mathrm{L} \\ y_\mathrm{L} \\ z_\mathrm{L} \end{pmatrix} = \mathbf{\Phi}_\varphi \begin{pmatrix} x_\mathrm{g} \\ y_\mathrm{g} \\ z_\mathrm{g} \end{pmatrix}. \quad (3)$$

This matrix is fully known from the experimental setting. The two coordinate systems coincide at zero goniometer setting.

The remaining problem addressed here is establishing the relation between the Cartesian coordinates of the reciprocal-lattice points and their *hkl* indices, which are the coordinates along the a^*, b^* and c^* axes. We employ the usual relation

$$\begin{pmatrix} x_\mathrm{g} \\ y_\mathrm{g} \\ z_\mathrm{g} \end{pmatrix} = \mathbf{CA} \begin{pmatrix} h \\ k \\ l \end{pmatrix}, \quad (4)$$

where the product **CA** is the orientation matrix, **A** is a crystallographic matrix describing the transformation between *hkl* indices and the Cartesian coordinates (in the goniometer-head-fixed coordinate system) for a crystal in an idealized setting, and **C** is an unknown rotation matrix relating the actual crystal orientation to the idealized setting. The matrix **A** is fully determined by the unit-cell parameters and an arbitrarily chosen idealized setting (described in Appendix *A*).

2.2. Laue diffraction model

With a polychromatic X-ray beam all reciprocal-lattice points within the resolution limits $1/d_\mathrm{res}$ and between the limiting Ewald spheres of radii $1/\lambda_\mathrm{min}$ and $1/\lambda_\mathrm{max}$ can in principle be recorded on a single image.

The Bragg condition can be written as

$$\mathbf{h}_i = (1/\lambda_i)(\mathbf{s}_i - \mathbf{s}^0), \quad (5)$$

where $\mathbf{s}^0$ and $\mathbf{s}_i$ are dimensionless unit vectors with directions aligned with the primary and diffracted beams, respectively, for spot i and λ_i is the wavelength. Both unit vectors and the Bragg angle θ_i are easily calculated from the experimental data in the laboratory coordinate system, and therefore also in the goniometer-head-fixed system. However, unlike in monochromatic X-ray diffraction or neutron time-of-flight measurements, in which the wavelength λ_i is known, in the case of X-ray Laue diffraction it is not possible to determine λ_i by experimental means given the current detector technology. Therefore $\mathbf{h}_i$ cannot be determined either. Thus derivation of the exact cell parameters and the unit-cell volume requires additional experimental information.

2.3. Laue data preprocessing

In order to be able to apply geometrical algorithms we use projections of $\mathbf{h}_i$ vectors onto a unit sphere,

$$\hat{\mathbf{h}}_i := \mathbf{h}_i / |\mathbf{h}_i|, \quad (6)$$

which can be calculated from the available data.

For each diffraction image, peak locations on the detector and their intensities as found by our new peak identification and integration method or by the *Precognition* program (Ren, 2010) are used to calculate $\hat{\mathbf{h}}_i$ in the laboratory coordinate system (see Appendix *A*; the new integration routine is to be described in a separate publication). Next, the $\mathbf{\Phi}_\varphi$ matrices for each image are used to transform all vectors into the goniometer-head-fixed coordinate system, effectively producing a single combined data set denoted as expt-Laue.

The collections of lattice points forming central-reciprocal-lattice rows will be referred to here as rays. When the coordinates of the observed peaks are transformed to the goniometer-head coordinate system all registrations from different frames having the same *hkl* indices but recorded at different λ should project exactly at the same point on the unit sphere. The same point on the unit sphere should also be shared by the other reciprocal lattice points located on the same ray. In practice, because of errors in the peak-center determination, arising from slight missettings, non-ideal spot shape, fixed pixel size or slight cell parameter variations, the experimentally determined $\hat{\mathbf{h}}$ vectors for a given *hkl* will form a cluster of points on the sphere located around the ideal position. Therefore the geometrical structure of the set of all $\hat{\mathbf{h}}_i$ vectors will be one of a collection of clusters of points distributed on the unit sphere, each cluster corresponding to an individual ray, as depicted in Fig. 1. In addition, spurious signals not resulting from Bragg diffraction (cosmic radiation, bad pixels and artefacts generated by the spot-finding algorithm) will

project as randomly distributed isolated points on the sphere with possibly significant intensity.

The number of experimental $\hat{\mathbf{h}}$ points in a cluster is the number of separate observations of the corresponding ray. It depends on the number of *hkl*s in a given ray within the resolution limit and on the geometrical relation of the ray to the goniometer axis. Usually the strongest reflections are low order and therefore the rays they belong to and the corresponding experimental clusters tend to be well populated.

2.4. The rotation matrix search strategy

A corresponding spherical pattern can be constructed from the cell parameters, Laue group and rays of reciprocal lattice points obtained from the monochromatic experiment. The problem of finding the rotation matrix $\mathbf{C}$ is equivalent to the problem of finding an optimal superposition of the two unit spheres such that points on the experimental sphere match points on the reference sphere. However, as the number of points to be matched between the monochromatic and Laue data sets can be of the order of tens of thousands a further reduction of data is necessary.

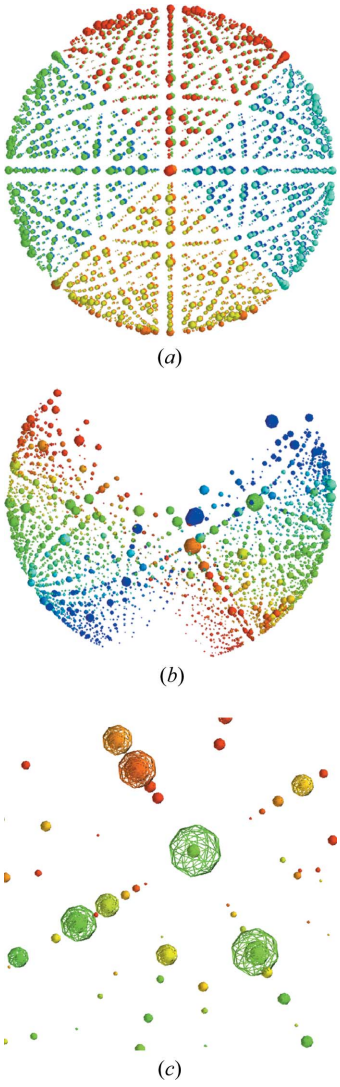

Figure 1
Visualization of projections of points in reciprocal space on a unit sphere for the CuIpip06 data set. Points are marked with small spheres in wireframe representation; the radius of each sphere is proportional to the square root of the reflection intensity. (*a*) Rays from monochromatic data sets; eight equivalent asymmetric units in reciprocal space are represented with different colors. (*b*), (*c*) Points from a Laue data set. The fraction of reciprocal space probed in this Laue data set can be deduced from (*b*). Points form clusters corresponding to rays as seen in the magnification in (*c*).

2.5. Clustering and filtering

Rather than working with all individual spots we search for clusters of $\hat{\mathbf{h}}$ vectors. Only the averaged $\langle\hat{\mathbf{h}}\rangle_i$ position for the *i*th cluster is used. Apart from reducing the computational cost of subsequent steps of the procedure, the clustering step allows for extra filtering of data: single points in the experimental data, not belonging to any cluster, even when possessing high intensity, have a high likelihood of being spurious effects, therefore only clusters with more than a selected number of experimental points are treated as groups of reliable reflections. The exact value depends on the measurement strategy. The smaller the φ spacing, the more populated should the clusters be, allowing for a higher cutoff value.

The routines commonly found in statistical libraries usually start with calculation of a distance matrix. In our case such a matrix is likely to be larger than the available computer memory, so a more subtle approach must be adopted. First a connectivity graph is constructed by identifying neighbors for each point. An algorithm based on space division and hash tables is used.

Then connected components of the graph are determined using the *NetworkX* software library (http://networkx.lanl.gov/). In the last step, hierarchical clustering using scipy.cluster.hierarchy (http://www.scipy.org/) functions is applied to points in each connected component separately and the final clusters are identified by cutting clustering hierarchy trees at a selected level. This level is expressed in terms of the largest allowed distance acceptable between points belonging to the cluster.

The best clusters are chosen by eliminating clusters with less than a minimum number of points and those with all spot intensities less than a given cutoff value. Depending on the data quality, the thresholds for the number of reflections in the cluster and the minimum accepted intensity may vary. The goal is to identify the 30–40 best clusters. A higher number increases the computational time of the superposition algorithm quadratically, while a smaller number decreases the chances of finding the proper rotation matrix.

As the rays are exactly known in the case of the monochromatic data set, no clustering operation is necessary. Instead, a simple intensity-based filtering is used to select 200–300 clusters with the most intense reflections.

A smaller number of points are selected in Laue measurements because usually a single-axis diffractometer is used with this technique, and thus only a fraction of the whole reciprocal space is probed. However, as it is impossible to say *a priori* which part of the reciprocal space is sampled, points must be

approximately uniformly selected from the whole reference data set.

2.6. The superposition algorithm

The stages of the rotation matrix search are illustrated in Fig. 2. The angles between all pairs of rays selected for matching are calculated for both the Laue and the monochromatic projections. Each angle between a pair of experimental rays defined by the selected clusters is then compared with each of the angles between monochromatic rays. (In the actual implementation a binary search in the array of sorted angles is used.) If the difference between the Laue and the monochromatic inter-ray angles falls within a set tolerance level, the fit is considered successful and the rotation matrix producing such overlay is stored. Each matrix can be represented by a point in the three-dimensional Euler space of rotation angles around three perpendicular axes.

Two inter-ray angles from Laue and monochromatic data sets can be accidentally similar; therefore there may be many occurrences of pairs of nearly identical angles. Assuming that the number of rays common in both data sets equals N, and that experimental errors fall within appropriate detection thresholds, there will be $N(N-1)/2$ pairs of rays giving nearly identical orientation matrices. In Euler space these matrices form a cluster of points, representing an agglomeration of very similar orientation matrices, embedded in a scattered distribution of a large number of random points, as illustrated in Fig. 3.

The same algorithm that searches for clusters of rays in the initial set of Laue data can also be successfully applied in Euler space to identify clusters of orientation matrices. Once an outstanding cluster is identified, a rotation matrix is calculated from the averaged Euler angles. In practice several equivalent clusters may occur in Euler space as a result of crystal symmetry. In this case an arbitrary selection can be made.

The whole rotation matrix search procedure with 200 monochromatic clusters and 35 experimental clusters can be completed in 5–7 min on a standard desktop computer (tests were run mostly on a Linux machine using a single core of an AMD Phenom II X6 1090 T processor).

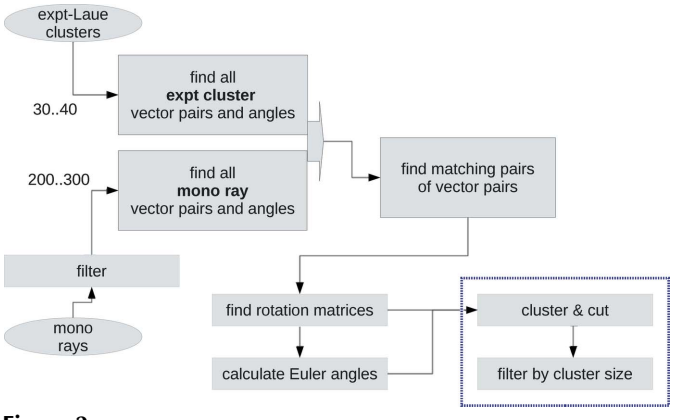

Figure 2
Schematic representation of the rotation matrix searching process.

2.7. Implementation: description of the *LaueUtil* toolkit

The treatment of the data described in the preceding section is performed by a series of programs belonging to the new toolkit, which is intended to provide an integrated solution for processing Laue diffraction data, in particular from pump–probe experiments.

The software is mostly written in the Python language; however, to assure sufficient speed of computation and input/output operations, it makes extensive use of Python extensions implemented in compiled languages, in particular NumPy and SciPy. The toolkit has a modular object-oriented design. It consists of a library of reusable software components (classes and functions) and executable scripts.

The cell parameters and structure factors resulting from the monochromatic experiment are read from a *SHELX*-compatible (Sheldrick, 2008) structure-factor file in .fcf format and converted to an HDF5 file. The intermediate and final results of computations are also stored in files in HDF5 format, which allows for direct inspection of all data with a broad choice of general purpose statistical and visualization programs capable of reading this format.

The programs are run from the command line, but some have an automatically generated graphical user interface (GUI) that allows users to set parameters for each computational step to be performed. The rotation matrix search program GUI allows visualization of the Euler space, interactive selection of any point and inspection of the corresponding rotation matrix.

The programs are available under a nonrestrictive, Mozilla Public License-like open-source license and can be downloaded from the SourceForge site (http://sourceforge.net/p/laueutil). Assistance with use of the programs is available from the authors.

3. Results

3.1. Test data

The method was applied to time-resolved Laue X-ray data collected at the 14-ID BioCars beamline at the Advanced

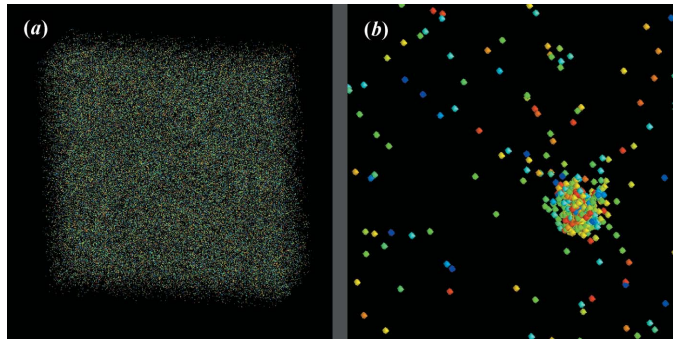

Figure 3
Visualization of a projection of Euler space. Each point represents a rotation matrix derived from two pairs of rays from Laue and monochromatic data sets with matching inter-ray angles. (*a*) Points are shown to fill the whole Euler space, which is a cuboid with dimensions $2\pi \times 2\pi \times \pi$. (*b*) A magnification showing a cluster containing over 460 points corresponding to a correct rotation matrix.

Table 1
Test data sets.

Compound short name	Crystallographic system	Space group	Cell parameters (Å, °)	Temperature (K)	No. of OFF data sets	No. of ON/OFF data sets
RhPNP	Monoclinic	$P2_1/c$	13.9783 (3), 20.2046 (5), 28.1465 (7), 90, 90.8420 (10), 90	225	1	1
CuIpip	Tetragonal	$P4_2/n$	14.5898 (5), 14.5898 (5), 7.5387 (2), 90, 90, 90	200	1	2
CuBF4M	Monoclinic	$P2_1/n$	12.0520 (10), 21.1930 (18), 17.2507 (14), 90, 93.952 (2), 90	180	6	9
CuBF4T	Triclinic	$P\bar{1}$	12.8340 (11), 17.4719 (15), 19.3926 (17), 106.466 (2), 99.421 (2), 95.440 (2)	180	8	18
CuTRI	Triclinic	$P\bar{1}$	10.9221 (10), 19.9498 (19), 20.3882 (19), 96.364 (2), 101.008 (2), 92.071 (2)	180	6	7

Photon Source, Argonne National Laboratory, in April 2011. Data for three different Cu^{I} bis(triphenylphosphine)phenanthroline salts, two with the BF_4 anion (triclinic and monoclinic polymorphs, referred to below as CuBF4T and CuBF4M, respectively) and one with the trifluoromethanesulfonate anion (CuTRI), were collected. A total of 17 crystals were used. The scans were performed either with or without laser exposure of the crystals (referred to as laser-ON and laser-OFF, respectively). Fifteen OFF-only scans and 34 ON/OFF scans with ON and OFF frames alternating were performed. The scans were collected with either 1 or 2° φ spacing between frames. The laser-to-X-ray pulse delays were set to 100 ns. No significant changes in crystallographic cell parameters were observed in the experiments.

In addition, the procedure was tested on data sets from a crystal of tetragonal $[Cu_4I_4(piperidine)_4]$ (Kamiński *et al.*, 2010) (referred to as CuIpip) and on the α modification of $[Rh_2(\mu\text{-PNP})_2(PNP)_2(BPh_4)_2]$ {PNP is $CH_3N[P(OCH_3)_2]_2$ and Ph is phenyl; Makal *et al.*, 2011} (referred to as RhPNP). Details of these data sets are summarized in Table 1. All data were collected at a 15 keV undulator setting, with an energy spread of $\Delta E/E \simeq 0.08$ (narrow band), yielding a resolution of ~0.9 Å. The minimum available crystal-to-detector distance was ~65 mm. The use of a 'pink' Laue beam combined with the restricted crystal-to-detector distance necessarily reduces the number of spots available on a single frame, thereby hampering single-image indexing procedures. However, this setting provides better spot separation and lower levels of diffuse scattering.

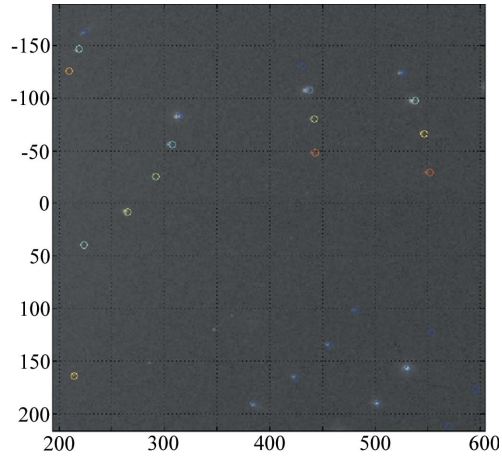

Figure 4
Overlay of predicted spot positions on a selected experimental image from the CuBF4T_07 data set, produced by the seed-skewness integration program *LaueGui* with an orientation matrix obtained with *LaueUtil*.

3.2. Assessment of the rotation matrix quality

For all data sets orientation matrices in qualitative agreement with the experimental pattern were obtained, as judged by visual inspection of the overlay of predicted spot positions on the experimental images (Fig. 4).

Two criteria were applied in order to test the quality of the orientation matrices. First, they were compared with the reference set of frame-by-frame-refined orientation matrices. This set was obtained with the *Precognition* refine (Ren, 2010) routine, which is a typical example of frame-by-frame macromolecule-oriented software. It is noticeable that, while the *Precognition* routine could be successfully applied to many of our data sets, it failed for a number of others, whereas the new methods were successful.

Subsequently the completeness of data integrated with the program *LaueGui* (Bolotovsky *et al.*, 1995; Messerschmidt & Tschentscher, 2008) using the matrices from *LaueUtil* were compared with the completeness of data obtained with the *Precognition* matrices.

3.2.1. Accuracy. The test was performed by multiplying the rotation matrix **C** by the inverse of the rotation matrix produced by *Precognition*, $\mathbf{C}_{\rm Prc}$, for individual frames:

$$\mathbf{M}_{\rm e} = \mathbf{C}\mathbf{C}_{\rm Prc}^{-1}. \qquad (7)$$

If the matrices **C** and $\mathbf{C}_{\rm Prc}$ were identical the product $\mathbf{M}_{\rm e}$ would be the identity matrix. In order to judge the deviations from identity, the matrix $\mathbf{M}_{\rm e}$ was converted into the set of three Euler angles. The average and maximum angular discrepancies are listed in Table 2 for a representative subset of data and in Table S1[1] for all data. These discrepancies are compared with the average discrepancies between the *Precognition* **C** matrices for individual frames and $\mathbf{C}_{\rm Prc}$ of the first indexed frame. The average discrepancies are very small, in the range of 0.05–0.30°, and can be chiefly attributed to the current absence of cell parameter refinement in the *LaueUtil* routine. Not surprisingly, more significant differences are

[1] Supplementary data for this paper are available from the IUCr electronic archives (Reference: AJ5180). Services for accessing these data are described at the back of the journal.

Table 2
Average and maximum angular discrepancies for selected data sets.

Data set	Type	Laser power (μJ mm^{-2})	φ spacing (°)	φ range (°)	*Precognition* average discrepancy (°)	*Precognition* maximum discrepancy (°)	*LaueUtil* average discrepancy (°)	*LaueUtil* maximum discrepancy (°)
CuBF4M_02								
Dark	OFF	0	2	91	0.100	0.223	0.152	0.216
Laserpower1	ON/OFF	0.4	1	21	0.087	0.158	0.087	0.158
Laserpower2	ON/OFF	0.6	1	21	0.052	0.085	0.059	0.132
Laserpower3	ON/OFF	0.8	1	21	0.067	0.107	0.114	0.140
Laserpower4	ON/OFF	1	1	21	0.187	0.230	0.102	0.130
Laserpower5	ON/OFF	1.2	1	21	0.215	0.343	0.099	0.192
CuBF4T_07								
Dark	OFF	0	1	91	0.116	0.222	0.149	0.247
Laser1	ON/OFF	0.9	1	91	0.157	0.272	0.111	0.196
Laser2	ON/OFF	1.1	2	91	0.119	0.230	0.154	0.204
CuIpip06								
Dark	OFF	0	1	91	0.100	0.174	0.071	0.152
Laser1	ON/OFF	0.6	1	91	0.090	0.120	0.044	0.065
Laser2	ON/OFF	0.8	1	51	0.120	0.190	0.140	0.280
RhPNP_27								
Dark	OFF	0	1	91	0.193	0.337	0.142	0.226
Laser1	ON/OFF	0.6	5	19	0.186	0.332	0.251	0.412

Table 3
Completeness statistics for selected laser-ON data sets.

	Precognition			*Precognition* (first frame)			*LaueUtil*		
	No. of reflections	Completeness (%)	R_{int}	No. of reflections	Completeness (%)	R_{int}	No. of reflections	Completeness (%)	R_{int}
CuBF4M_02									
Laserpower1	1600	27.7	0.054	1424	24.8	0.054	1551	26.9	0.045
Laserpower2	1601	27.8	0.048	1544	26.8	0.071	1586	27.2	0.049
Laserpower3	1572	27.5	0.049	1516	26.3	0.048	1555	27.1	0.049
Laserpower4	1498	27	0.052	1449	25.2	0.056	1485	25.9	0.049
Laserpower5	1488	26.4	0.055	1272	23.1	0.053	1320	24.1	0.055
CuBF4T_07									
Laser1	6103	56.9	0.041	5251	49.7	0.038	6050	57.1	0.038
Laser2	5679	52.8	0.049	5311	49.5	0.052	5327	49.7	0.051
CuIpip06									
Laser1	841	82.2	0.072	842	80.3	0.070	836	81.7	0.072
Laser2	549	55.1	0.102	560	53.6	0.102	546	50.8	0.098
RhPNP_27									
Laser1	1955	20.9	0.087	1583	15.9	0.074	1632	16.4	0.079

observed for the frames collected with laser exposure. This can be attributed to a greater chance of crystal shift on the mount due to heating and in principle to small cell parameter changes. We could not find a **C** matrix suitable for the complete data set in two cases in which a the crystal shifted by more than 4° during data collection (data sets CuBF4T_04 and CuTRI_02 in the supporting material).

When the shift is no larger than a few degrees, a preliminary rotation matrix can be refined on a frame-by-frame basis, a routine for which is currently being developed together with a procedure for the indexing of the individual reflections. The higher the crystallographic symmetry, the better the agreement with the reference results. Typical variations of the angular discrepancy between the *Precognition*-derived and the *LaueUtil*-derived **C** matrices are illustrated in Fig. 5.

On one occasion (data set CuBF4T_10 in the supporting material), an initial failure of the new method occurred because of the use of incorrect monochromatic reference data from a CuBF4M sample. In this case, the complete lack of any clusters in visualization of the Euler space suggested the cause of the problem. On the other hand, in cases in which cell parameters for the right compound but at the wrong temperature (hence differing by about 0.3 Å or 1° from the correct parameters) were applied, the current method performed well and did not require adjustments in the cluster-defining parameters.

3.2.2. Resulting data completeness. The data were integrated in *LaueGui* and processed for application of the RATIO method (Coppens *et al.*, 2009). For photocrystallographic purposes, only laser-exposed data sets were included. These data are the most sensitive to inaccuracies of the initial orientation matrix. The data were integrated using (*a*) *Precognition*-derived orientation matrices on a frame-by-frame basis, (*b*) a single *Precognition*-derived orientation matrix from the first experimental frame only and (*c*) a *LaueUtil*-derived average orientation matrix. The resulting completeness and *R* values are compared in Table 3.

The *LaueUtil*-derived orientation matrix yields data sets of comparable quality and a completeness within 4% (and usually less) of those obtained by using orientation matrices adjusted on a frame-by-frame basis, with a gain in data processing time and ease of use (the *LaueUtil*-derived orientation matrix could be found in a few minutes, in contrast with a few hours spent with software using the frame-by-frame approach). In most cases, the average global orientation matrix yields a better fit than a single-frame-adjusted orientation matrix.

4. Conclusions

Provided that the crystal does not move on its mount during the experiment and that the cell parameters of the sample are known and do not change significantly during data collection, the method developed yields the averaged orientation matrix

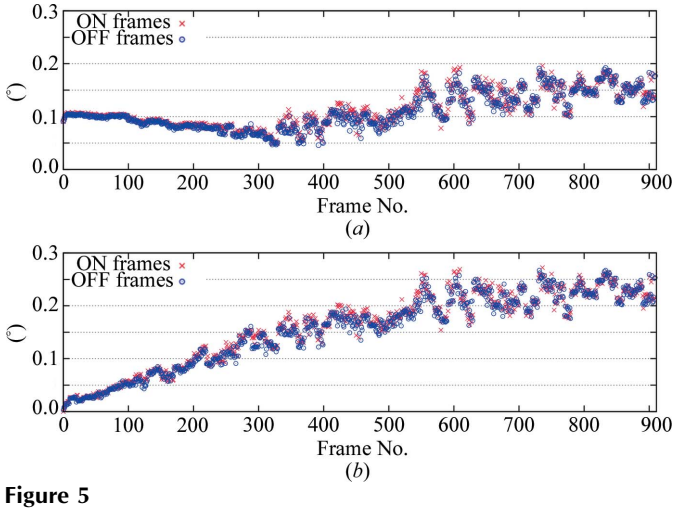

Figure 5
Plots comparing the angular discrepancy between the refined rotation matrices for each frame and (*a*) the matrix obtained with *LaueUtil* and (*b*) a matrix arbitrarily selected (the first one) from the set of the matrices refined with the *Precognition* program. The values are the maximum of absolute values of Euler angles calculated with equation (3). Results for frames with (ON) and without (OFF) laser expositions are marked with different point styles.

giving the best fit to the collected frames. It is applicable to small and medium unit-cell crystals for which methods developed specifically for macromolecular crystallography are often not applicable. The matrices are suitable for direct integration of the data. The maximum discrepancies with matrices from the *Precognition* program (Ren, 2010) are found to be in the range of 0.05–0.25°. The completeness of integrated data is very close to that obtained with frame-by-frame-refined cell parameters and orientation matrices, with a considerable gain in data processing time and ease of use. In time-resolved pump–probe experiments, the samples are subject to laser exposure, and therefore crystal cell parameter and crystal orientation changes are more likely. Even in such cases the method provides orientation matrices suitable for direct integration, with the loss of data generally not exceeding 2%. In the remaining cases a 'best' matrix fitting most of the experimental frames is suitable as an input for matrix orientation/cell parameter refinement in a number of available programs.

APPENDIX *A*
The geometry of the experiment

The laboratory coordinate system used in the method uses the following convention: it is anchored at the crystal position, the X axis points towards the X-ray source and is parallel to the X-ray beam, while the horizontal Y and vertical Z axes are parallel to the detector plane such that the coordinate system is right handed. This definition is as initially defined by Arndt & Wonacott (1977) and described by Carr *et al.* (1992) but, we note, different from the one utilized by Ravelli *et al.* (1996), in which the Z axis coincided with the incident beam. The crystal-to-detector distance will be denoted as d, while z and y are the vertical and horizontal coordinates of a reflection relative to the direct beam position on the detector.

The X-ray beam coincides with the X axis of the laboratory coordinate system. From the position (X_i, Y_i) of each spot i on the detector and the crystal-to-detector distance d, the Bragg angle θ_i is found as

$$\theta_i = \tfrac{1}{2}\arctan\left[(X_i^2 + Y_i^2)^{1/2}/d\right], \tag{8}$$

and $\mathbf{s}_i^0$ and $\tilde{\mathbf{s}}_i$ are defined as

$$\mathbf{s}^0 = (-1, 0, 0), \tag{9}$$

$$\tilde{\mathbf{s}}_i = (-d, -X_i, Y_i), \tag{10}$$

$$\mathbf{s}_i = \tilde{\mathbf{s}}_i/|\tilde{\mathbf{s}}_i|, \tag{11}$$

where we also note a rotation from the image file coordinate system to the laboratory system.

The $\mathbf{\Phi}_\varphi$ matrix describing the rotations of the goniometer head takes the following form:

$$\mathbf{\Phi}_\varphi = \begin{pmatrix} \cos\varphi & \sin\varphi & 0 \\ -\sin\varphi & \cos\varphi & 0 \\ 0 & 0 & 1 \end{pmatrix}. \tag{12}$$

The matrix $\mathbf{A}$ is fully determined by unit-cell parameters and an arbitrarily chosen idealized setting in which $\mathbf{c}^*$ is parallel to the Z axis and $\mathbf{a}^*$ lies in the XZ plane with positive x component. It follows that $\mathbf{a}$ is parallel to the X axis. The full form of $\mathbf{A}$ is calculated using standard crystallographic expressions (Giacovazzo *et al.*, 2002) from the corresponding definition of real-space unit-cell vectors as $\mathbf{a} = (a, 0, 0)$, $\mathbf{b} = (b\cos\gamma, b\sin\gamma, 0)$ and $\mathbf{c} = (c\cos\beta, -c\sin\beta\cos\alpha^*, 1/c^*)$:

$$\mathbf{A} = \begin{pmatrix} a^*\sin\beta^* & -b^*\sin\alpha^*\cos\gamma^* & 0 \\ 0 & b^*\sin\alpha^*\sin\gamma^* & 0 \\ a^*\cos\beta^* & -b^*\cos\alpha^* & c^* \end{pmatrix}. \tag{13}$$

Support of this work by the National Science Foundation (grant No. CHE0843922) is gratefully acknowledged. Use of the BioCARS Sector 14 was supported by the National Institutes of Health, National Center for Research Resources, under grant No. RR007707. The Advanced Photon Source is supported by the US Department of Energy, Office of Basic Energy Sciences, under contract No. W-31-109-ENG-38. The cell parameters and structure factors from monochromatic experiments for three Cu^I bis(triphenylphosphine)phenanthroline salts were kindly supplied by Dr Jason B. Benedict.

References

Anderson, S., Srajer, V., Pahl, R., Rajagopal, S., Schotte, F., Anfinrud, P., Wulff, M. & Moffat, K. (2004). *Structure*, **12**, 1039–1045.
Arndt, U. W. & Wonacott, A. J. (1977). *The Rotation Method in Crystallography*. Amsterdam: North Holland.
Bolotovsky, R., White, M. A., Darovsky, A. & Coppens, P. (1995). *J. Appl. Cryst.* **28**, 86–95.
Campbell, J. W. (1995). *J. Appl. Cryst.* **28**, 228–236.
Carr, P. D., Cruickshank, D. W. J. & Harding, M. M. (1992). *J. Appl. Cryst.* **25**, 294–308.
Coppens, P. (2011). *J. Phys. Chem. Lett.* **2**, 616–621.

Coppens, P., Pitak, M., Gembicky, M., Messerschmidt, M., Scheins, S., Benedict, J., Adachi, S., Sato, T., Nozawa, S., Ichiyanagi, K., Chollet, M. & Koshihara, S. (2009). *J. Synchrotron Rad.* **16**, 226–230.
Giacovazzo, C., Monaco, H. L., Artioli, G., Viterbo, D., Ferraris, G., Gilli, G., Zanotti, G. & Catti, M. (2002). *Fundamentals of Crystallography*. New York: Oxford University Press.
Gupta, V. K. & Agnew, S. R. (2009). *J. Appl. Cryst.* **42**, 116–124.
Hart, H. V. & Rietman, E. A. (1982). *J. Appl. Cryst.* **15**, 126–129.
Helliwell, J. R., Habash, J., Cruickshank, D. W. J., Harding, M. M., Greenhough, T. J., Campbell, J. W., Clifton, I. J., Elder, M., Machin, P. A., Papiz, M. Z. & Zurek, S. (1989). *J. Appl. Cryst.* **22**, 483–497.
Jacobson, R. A. (1986). *J. Appl. Cryst.* **19**, 283–286.
Kamiński, R., Graber, T., Benedict, J. B., Henning, R., Chen, Y.-S., Scheins, S., Messerschmidt, M. & Coppens, P. (2010). *J. Synchrotron Rad.* **17**, 479–485.
Laughier, J. & Filhol, A. (1983). *J. Appl. Cryst.* **16**, 281–283.
Makal, A., Trzop, E., Sokolow, J., Kalinowski, J., Benedict, J. & Coppens, P. (2011). *Acta Cryst.* A**67**, 319–326.
Messerschmidt, M. & Tschentscher, T. (2008). *Acta Cryst.* A**64**, C611.
Moffat, K. (2001). *Chem. Rev*. **101**, 1569–1581.
Ravelli, R. B. G., Hezemans, A. M. F., Krabbendam, H. & Kroon, J. (1996). *J. Appl. Cryst.* **29**, 270–278.
Ren, Z. (2010). *Precognition User Guide.* RenZ Research Inc., Illinois, USA.
Sheldrick, G. M. (2008). *Acta Cryst.* A**64**, 112–122.
Šrajer, V., Crosson, S., Schmidt, M., Key, J., Schotte, F., Anderson, S., Perman, B., Ren, Z., Teng, T., Bourgeois, D., Wulff, M. & Moffat, K. (2000). *J. Synchrotron Rad.* **7**, 236–244.
Wenk, H. R., Heidelbach, F., Chateigner, D. & Zontone, F. (1997). *J. Synchrotron Rad.* **4**, 95–101.